



POLITECNICO DI TORINO  
Repository ISTITUZIONALE

Propagation of toxic substances in the urban atmosphere: A complex network perspective

*Original*

Propagation of toxic substances in the urban atmosphere: A complex network perspective / Fellini, Sofia; Salizzoni, Pietro; Soulhac, Lionel; Ridolfi, Luca. - In: ATMOSPHERIC ENVIRONMENT. - ISSN 1352-2310. - ELETTRONICO. - 198(2019), pp. 291-301.

*Availability:*

This version is available at: 11583/2716997 since: 2018-11-11T12:35:31Z

*Publisher:*

Elsevier

*Published*

DOI:10.1016/j.atmosenv.2018.10.062

*Terms of use:*

openAccess

This article is made available under terms and conditions as specified in the corresponding bibliographic description in the repository

*Publisher copyright*

elsevier

-

(Article begins on next page)

Atmospheric Environment

Elsevier Editorial System(tm) for

Manuscript Draft

Manuscript Number:

Title: Propagation of toxic substances in the urban atmosphere: a complex network perspective

Article Type: Research Paper

Keywords: Urban air pollution; Street network; Complex networks; Vulnerability; Accidental releases; Spreading on networks.

Corresponding Author: Miss Sofia Fellini, M.Eng.

Corresponding Author's Institution: POLITECNICO DI TORINO

First Author: Sofia Fellini, M.Eng.

Order of Authors: Sofia Fellini, M.Eng.; Pietro Salizzoni; Lionel Soulhac; Luca Ridolfi

Abstract: The accidental or malicious release of toxic substances in the urban atmosphere is a major environmental and safety problem, especially in large cities. Computational fluid dynamics codes and simplified modelling tools have been used in the last decades to model pollutant dispersion in urban areas. These studies have shown that propagation is strongly influenced by the layout of buildings and, therefore, by the street topology of the city. This work presents a novel approach to the study of toxic propagation within the urban canopy based on the theory of complex networks. Following recent studies on the development of urban dispersion models, the urban canopy is modelled as a network: the streets and the street intersections represent respectively the links and the nodes of the network. The direction and the weights of the links contain the geometric characteristics of the street canyons and their wind conditions. Within this approach, propagation is modelled as a spreading process on networks and a depth-first search algorithm is used to rapidly delimit the zone of influence of a source node. This zone is the set of streets that are contaminated from the source. As a case study, the proposed model is applied to the urban tissue of the city of Lyon. The algorithm simulates a toxic release in all the nodes of the network and identifies the number of people affected by each propagation process. In this way, vulnerability maps of the city are constructed. Moreover, various wind and concentration scenarios are easily implemented. These results evidence how the proposed method is effective for the rapid assessment of the most vulnerable points in a city, avoiding the use of long numerical simulations.



**POLITECNICO  
DI TORINO**

Department of  
Environment, Land and  
Infrastructure Engineering

Torino, July 16, 2018

To:  
Editorial Board of Atmospheric Environment

Subject: Manuscript Submission

Dear Editor,

we are enclosing herewith the manuscript entitled "Propagation of toxic substances in the urban atmosphere: a complex network perspective" for consideration of publication in Atmospheric Environment. With the present submission, we undertake the responsibility that the above-mentioned manuscript is original and has not been published nor is currently under consideration for publication elsewhere.

The research reported in this manuscript proposes an innovative approach for the study of pollutant dispersion within the urban canopy. This new approach is based on the promising theory of complex networks and allows us to model propagation from a source point as a spreading process on networks. In this way, the area of a city affected by a toxic release can be delimited with very low computational costs and vulnerability maps of urban areas can be rapidly constructed.

Our research is of interest for many disciplines, from urban meteorology to complex network science, and makes a significant step forward in the field of atmospheric fluid dynamics. Moreover, our methodology provides interesting tools for relevant current issues like urban pollution mitigation and terrorism prevention. We are thus confident that it is appropriate for publication in Atmospheric Environment.

All authors approved the manuscript and this submission. We know of no conflicts of interest associated with this publication. For any further clarification, do not hesitate to contact us.

We wish to thank you for your consideration and attention.

Best Regards,

Sofia Fellini  
Pietro Salizzoni  
Lionel Soulhac  
Luca Ridolfi

1 Propagation of toxic substances in the urban  
2 atmosphere: a complex network perspective

3 Sofia Fellini<sup>a,b,\*</sup>, Pietro Salizzoni<sup>b</sup>, Lionel Souhac<sup>b</sup>, Luca Ridolfi<sup>a</sup>

4 <sup>a</sup>*Department of Environmental, Land, and Infrastructure Engineering, Politecnico di  
5 Torino, Corso Duca degli Abruzzi 24, 10129 Turin, Italy*

6 <sup>b</sup>*Laboratoire de Mécanique des Fluides et d'Acoustique, UMR CNRS 5509, Université de  
7 Lyon, Ecole Centrale de Lyon, INSA Lyon, Université Claude Bernard Lyon I, 36, avenue  
8 Guy de Collongue, 69134 Ecully, France*

---

9 **Abstract**

10 The accidental or malicious release of toxic substances in the urban atmo-  
11 sphere is a major environmental and safety problem, especially in large cities.  
12 Computational fluid dynamics codes and simplified modelling tools have been  
13 used in the last decades to model pollutant dispersion in urban areas. These  
14 studies have shown that propagation is strongly influenced by the layout of  
15 buildings and, therefore, by the street topology of the city. This work presents  
16 a novel approach to the study of toxic propagation within the urban canopy  
17 based on the theory of complex networks. Following recent studies on the devel-  
18 opment of urban dispersion models, the urban canopy is modelled as a network:  
19 the streets and the street intersections represent respectively the links and the  
20 nodes of the network. The direction and the weights of the links contain the ge-  
21 ometric characteristics of the street canyons and their wind conditions. Within  
22 this approach, propagation is modelled as a spreading process on networks and  
23 a depth-first search algorithm is used to rapidly delimit the zone of influence of  
24 a source node. This zone is the set of streets that are contaminated from the  
25 source. As a case study, the proposed model is applied to the urban tissue of  
26 the city of Lyon. The algorithm simulates a toxic release in all the nodes of  
27 the network and identifies the number of people affected by each propagation  
28 process. In this way, vulnerability maps of the city are constructed. Moreover,  
29 various wind and concentration scenarios are easily implemented. These results

---

\*Corresponding author  
Preprint submitted to *Environmental Modelling & Software* (Sofia Fellini)

30 evidence how the proposed method is effective for the rapid assessment of the  
31 most vulnerable points in a city, avoiding the use of long numerical simulations.  
32 *Keywords:* Urban air pollution, Street network, Complex networks,  
33 Vulnerability, Accidental releases, Spreading on networks

---

## 34 **1. Introduction**

35 Large cities are particularly vulnerable to air pollution as they exhibit both a  
36 large number of potential sources and a high density of people exposed (Brunekreef  
37 and Holgate, 2002; Heinrich and Wichmann, 2004). Urban air pollution is  
38 mainly linked to human activities and in particular to vehicular traffic, heating of  
39 buildings and industrial emissions (Mayer, 1999). Moreover, accidental releases  
40 such those related to gas leaks, industrial plants or the transport of dangerous  
41 goods are particularly critical in densely populated environments. Besides un-  
42 intentional releases, the current political situation also raises the possibility of  
43 terrorist attacks aimed at the dispersal of toxic or pathogenic substances in the  
44 air (Tucker, 2000; McLeish, 2017).

45 For these reasons, local administrations are urged to adopt not only instru-  
46 ments for air quality control but rather predictive tools for the management of  
47 dangerous situations due to accidental and malicious releases. These actions are  
48 in line with the current challenge of building resilient metropolises able to cope  
49 with emergencies (Berke et al., 2009; Ahern, 2011).

50 Dispersion models are commonly used to predict urban pollution and to es-  
51 timate concentration of toxic substances. Computational fluid dynamics (CFD)  
52 simulations are the most suitable tool for modelling dispersion in a complex  
53 geometry like the urban fabric, since they solve the velocity and concentration  
54 field in the whole domain (Blocken, 2015). However, these models require a huge  
55 computational cost and therefore long simulation times and high performance  
56 computers. To reduce the computational cost, several modelling approaches  
57 have been developed in the last decades (Di Sabatino et al., 2013). These in-  
58 clude street network models (e.g., Carruthers et al., 2000; Soulhac et al., 2011)

59 based on a simplified description of the building geometry and modelling the  
60 mass exchange within and above the urban canopy by parametrising few key  
61 transfer processes. Their formulation rely on the basic idea that the urban  
62 structure of the city, the orientation of the streets and their connectivity play a  
63 major role in determining the intensity of these transfer processes.

64 Starting from these considerations, this work presents a novel approach for  
65 the study of toxic pollutant dispersion within the urban canopy. The aim is  
66 to evaluate rapidly and with negligible computational cost the vulnerability  
67 of a dense city to the release of harmful airborne pollutants by means of the  
68 modern techniques provided by the theory of complex network. According to  
69 this perspective, propagation phenomena in the streets are represented as a  
70 transport process on a network.

71 In complex network theory (e.g., Boccaletti et al., 2006; Newman, 2010),  
72 complex systems are traced back to a set of entities (nodes) that interact with  
73 each other. Interactions are represented as links between the nodes and may  
74 have weights that describe the strength of these interactions. Complexity does  
75 not lie in the elements that form the system, but rather in their topology and  
76 within the pattern of their interconnections. In the last few years, the theory of  
77 complex networks has gained a great attention in countless fields, from the social  
78 sciences (e.g., Borgatti et al., 2009) to engineering (e.g., Carvalho et al., 2009;  
79 Yazdani and Jeffrey, 2011; Giustolisi and Ridolfi, 2014). Recently, a network  
80 approach has been adopted for the description of geophysical fluid motion and  
81 associated transport phenomena. Gelbrecht et al. (2017) propose a complex  
82 network representation of wind flows to study regional meteorology systems,  
83 while Ser-Giacomi et al. (2015) represent mixing and dispersion processes in the  
84 Mediterranean as a transportation network.

85 In this work we focus on the pollutant dispersion at the local urban scale.  
86 The topology of the city is modelled as a network, within which the propagation  
87 of the airborne toxic pollutant occurs. The streets and the street intersections  
88 are respectively the links and the nodes of the network. The direction and the  
89 weight of the links contain the fluid-dynamics properties of the flow within the

90 streets and the geometric characteristics of the bordering buildings. In this  
91 way, the topology of the city and the wind conditions along the streets are all  
92 represented in a single mathematical structure, that is a weighted and directed  
93 complex network. Given an initial point, i.e. a pollutant source, the pathways  
94 of propagation along the streets can be immediately predicted by this schematic  
95 representation. In particular, as in epidemics applications (Newman, 2002), a  
96 search algorithm on networks is adopted to delimit the zone of influence of a  
97 source node, that we define as the part of the network affected by toxic propa-  
98 gation. By applying this procedure to each node in the network, vulnerability  
99 maps can be easily constructed and the urban areas with the highest spreading  
100 potential are revealed at a glance. The method is fast and can be applied to  
101 entire cities with a low computational cost.

102 The final aim is to provide a reliable and rapid method to (i) identify the  
103 most vulnerable points in the city, i.e. the source points from which the toxic  
104 spreading can affect the greatest number of people, and (ii) to understand the  
105 effect of wind conditions on urban vulnerability. To this purpose, the method-  
106 ological tools of network analysis are adopted and long numerical simulation of  
107 dispersion processes are avoided.

108 The work is organized as follows. In Section 2, we describe the physical as-  
109 sumptions adopted to model pollutant propagation in the urban canopy. Then,  
110 the network perspective is introduced in Section 3. The basic steps to con-  
111 struct the street network and its weight matrices are thus described and the  
112 algorithm for spreading on networks is presented. Subsequently, the proposed  
113 general method is applied to the city of Lyon (France). Vulnerability maps  
114 for a district of Lyon are shown and analysed in Section 4. Finally, the main  
115 conclusions obtained from the presented work are summarized.

116 **2. Physical assumptions about the propagation of a toxic substance**  
117 **in the urban environment**

118 Transport and mixing processes in the urban environment are characterized  
119 by complex fluid structures due to the interaction between the atmospheric  
120 flow and the city. The presence of buildings and vegetation highly affects the  
121 structure of the urban boundary layer, characterized by the generation of a  
122 shear layer at the top of the canopy, wake diffusion behind buildings, and form  
123 drag due to the pressure differences across the roughness elements (Roth, 2000).  
124 Moreover, the flow field in the streets is altered by the convective fluxes due  
125 to the differential solar irradiance on building walls and to the heat sources  
126 related to human activities (Oke, 1982; Arnfield, 2003). The simulation of all  
127 these dynamical effects on the flow field within the urban canopy is nowadays a  
128 challenge for modellers that adopt sophisticated computational tools, typically  
129 CFD codes (Tominaga and Stathopoulos, 2012). These require a huge amount of  
130 input data and high computational costs, which limit their use when analysing  
131 a large number of emission scenarios. In this latter case, alternative simulation  
132 strategies should be adopted, based on a simplified description of the flow and  
133 of the dispersion phenomena occurring within the urban fabric.

134 The physical assumptions for the propagation model presented in this work  
135 are based on a street network approach (e.g., Namdeo and Colls, 1996; Soulhac  
136 et al., 2011). The geometry of the urban canopy is simplified to a network of  
137 streets (Fig. 1.a), and the streets are represented as urban canyons, i.e. cavities  
138 of rectangular section with length  $l$ , height  $h$  and width  $w$  (Fig. 1.b). Following  
139 the approach of Soulhac et al. (2011), the main transport phenomena for a  
140 airborne pollutant in the urban canopy are (i) the convective mass transfer  
141 along the street due to the mean wind along the longitudinal axis, (ii) the  
142 vertical transfer toward the external atmosphere and (iii) the transport at street  
143 intersections.

144 We introduce here two further simplifications to this approach. The first  
145 concerns the model for the pollutant transfer at street intersections, which is



146 significantly different from that adopted by Soulhac et al. (2011). Secondly,  
 147 we will neglect the dispersion occurring above roof level. Since our focus is  
 148 on ground level releases only (therefore inducing maximal concentration at the  
 149 street level, within the canopy), we will assume that the amount of pollutant  
 150 transferred out of the streets, towards the overlying boundary layer, will not  
 151 further contribute to the pollutant concentration in the downwind streets. In  
 152 other words, we consider that this vertical flux of pollutants, from the canopy  
 153 to to the external atmosphere, will induce negligible concentrations above roof  
 154 level (due to the high dilution occurring in the lower part of the boundary layer,  
 155 compared to that within the streets) and that eventual mass flows from the  
 156 overlying atmosphere towards the street canyons will not contribute significantly  
 157 to ground level pollution. These two assumptions allow us to adapt the street  
 158 network approach to the propagation model presented in Section 3 based on the  
 159 formalism of the theory of complex networks.

160 In the following, the transport mechanisms along a street canyon and at  
 161 street intersections are described in details. The emission scenario consists of  
 162 a ground level and punctual release ( $s$  in Fig. 1) within the urban canopy.  
 163 The external wind blowing on the city with direction  $\Phi$  is the driving force for  
 164 propagation processes.

### 165 *2.1. Transport along a street canyon*

166 Consider a source  $s$  releasing a gaseous substance that results in a concen-  
 167 tration  $c_0$  at the beginning of a street canyon, as illustrated in Fig. 1.b-c. The  
 168 substance propagates horizontally due to the advective flux along the longitu-  
 169 dinal axis, and vertically due to the turbulent flux between the street and the  
 170 overlying atmosphere (Soulhac et al., 2013). A simple but exhaustive way to  
 171 model these two mechanisms is the use of the one-dimensional transport equa-  
 172 tion

$$\frac{\partial c}{\partial t} + u_{st} \frac{\partial c}{\partial x} + \frac{u_d}{h} (c - c_{ext}) = 0, \quad (1)$$

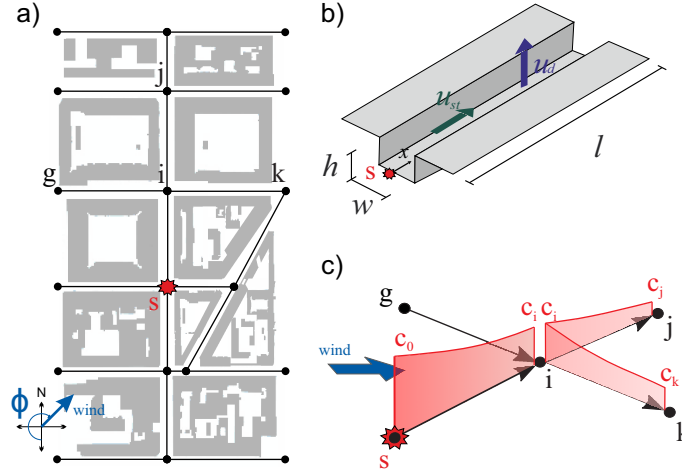


Figure 1: a) Toxic source  $s$  within a network of streets. Propagation is driven by the wind blowing on the city with direction  $\Phi$ . b) Representation of a street canyon with the main variables of the model. c) Transport of a contaminated flow in street intersections.

173 whose solution is the function  $c(x, t)$ , i.e. the concentration along the longitu-  
 174 dinal coordinate  $x$  over time  $t$ .

175 The first two terms in (1) describe the convective transport driven by the  
 176 spatially averaged wind velocity along  $x$  ( $u_{st}$ ). This velocity is assumed to  
 177 be given by a balance between the stress imposed at the canopy top by the  
 178 external atmospheric flow and the drag due to the roughness of the canyon walls  
 179 (neglecting the role of pressure gradients). Under this assumption, Soulhac  
 180 et al. (2008) derived an analytical formulation for  $u_{st}$ , as a function of the  
 181 external wind intensity and direction, the geometry of the street canyon and the  
 182 aerodynamic roughness of building walls (see Appendix A). The third term in (1)  
 183 models the mass transfer from/to the canyon to/from the overlying atmosphere  
 184 by means of a bulk exchange velocity  $u_d$  (Salizzoni et al., 2009) estimated as

$$u_d = \frac{u_*}{\sqrt{2\pi}}, \quad (2)$$

185 where  $u_*$  is the friction velocity of the overlying boundary layer flow. Assuming  
 186 that pollutant concentration above the canopy,  $c_{ext}$ , is negligible compared to  
 187 the concentration in the canyon, the vertical flux is unidirectional. This vertical

188 loss is the only decay term in the model, since it is assumed that the involved  
189 toxic substances do not undergo chemical or biological transformations or, in  
190 any case, have a reaction time longer than the time needed for propagation.

191 In (1), turbulent longitudinal diffusion is not considered as it is negligible  
192 with respect to the longitudinal advection.

193 Equation (1) was solved for both an instantaneous and a continuous release  
194 in the source (see Appendix B). In the first case, the initial condition is set  
195 as a rectangular pulse with height  $c_0$ . The solution describes this initial step  
196 travelling along the street with velocity  $u_{st}$  and undergoing an exponential decay  
197 of concentration. In the second case, the initial condition is a continuous release  
198 with constant concentration  $c_0$ . The solution is a front that spreads along the  
199 street with velocity  $u_{st}$ . Although the analytical solutions are different, the  
200 concentration at the end of the street ( $x = l$ ) in both cases is the same:

$$c_l \left( x = l, t = \frac{l}{u_{st}} \right) = c_0 e^{-\frac{l}{u_{st}} \frac{u_d}{h}}. \quad (3)$$

201 Thus, the concentration at the beginning of the street ( $c_0$ ) undergoes an expo-  
202 nential decay driven by the ratio between the advection time ( $l/u_{st}$ ) that the  
203 toxic front spends to reach the end of the street, and the vertical transfer time  
204 ( $h/u_d$ ). The terms in the exponent summarize all the information about the  
205 geometry of the canyon and the flow dynamics in it.

## 206 *2.2. Transport in the street intersections*

207 The flow field in the street intersections is driven by complex physical pro-  
208 cesses that depend on multiple geometric and meteorological parameters. Sev-  
209 eral studies (e.g. Hunter et al., 1990; Robins et al., 2002; Soulhac et al., 2009)  
210 have demonstrated that even slight variations in the building geometry and wind  
211 direction can affect significantly the redistribution of the incoming fluxes over  
212 the outgoing fluxes. On the basis of these observations, Soulhac et al. (2009)  
213 have developed a model, quantifying the balance of the time-averaged incoming  
214 and outgoing fluxes at the street intersection, depending on its geometry and

215 on the direction of the external wind. In defining the exchange model in the  
 216 intersection for the pollutant propagation within the network we however adopt  
 217 a different approach. Our aim is twofold: i) adopt a model which is the simplest  
 218 as possible, and ii) adopt a conservative approach. With these aims we will con-  
 219 sider that the concentration of pollutants at the beginning of the streets exiting  
 220 the intersection is the one at the end of the incoming contaminated canyon.

221 Consider a simple intersection with a single incoming and one outgoing street  
 222 canyon. The air flow entering the intersection with a concentration  $c_{in}$  is  $Q_{in}$ ,  
 223 while the air flow outgoing the intersection with a concentration  $c_{out}$  is  $Q_{out}$ .  
 224 Two cases are possible for the mass balance in the intersection. In the first  
 225 case, the mass flow from the incoming canyon ( $\dot{m}_{in} = c_{in}Q_{in}$ ) is lower than the  
 226 mass flow toward the outgoing canyon ( $\dot{m}_{out} = c_{out}Q_{out}$ ). In order for the mass  
 227 balance to be satisfied, an external mass flow ( $\dot{m}_{ext}$ ) from the atmosphere above  
 228 the canopy enters the intersection vertically with an air flow rate  $Q_{ext}$  and a  
 229 concentration  $c_{ext}$ . Since it is assumed that the external concentration  $c_{ext}$  is  
 230 negligible, this mass flow makes a zero contribution in the mass balance and  $c_{out}$   
 231 is given by  $c_{out} = c_{in}Q_{in}/Q_{out}$ . As the flow rate balance in the intersection is  
 232  $Q_{in} + Q_{ext} = Q_{out}$ , the ratio  $Q_{in}/Q_{out}$  is lower than 1 and thus  $c_{out} < c_{in}$ . In the  
 233 second case,  $\dot{m}_{in} > \dot{m}_{out}$  and the flow  $\dot{m}_{ext}$  leaves the intersection vertically.  
 234 We consider that the concentration leaving the intersection is the same for  
 235 both the upwards flow and the flow towards the outgoing street canyon, i .e.  
 236  $c_{ext} = c_{out}$ . Applying the mass ( $c_{in}Q_{in} = c_{out}Q_{out} + c_{ext}Q_{ext}$ ) and flow rate  
 237 ( $Q_{in} = Q_{out} + Q_{ext}$ ) balance equations, we find that  $c_{out} = c_{in}$ . These arguments  
 238 therefore show that our approach is conservative, i.e. tends to maximise the  
 239 pollutant concentration in the downwind streets.

240 Similarly, in case of several streets crossing, we will affect the same concen-  
 241 tration at the upwind section of all streets placed downwind the intersection. In  
 242 other words, we are assuming that the pollutant puff reaching the intersection  
 243 from a generic street will have a same probability of entering in any of the streets  
 244 placed downwind the intersection. In doing so, we will consider the trajectories  
 245 of all possible paths of the pollutant puffs that travel downwind their emission

246 point.

247 The assumptions adopted for the transport in street intersections are clearly  
248 illustrated in Fig.1c. The contaminated flow from street  $(s, i)$  propagates to-  
249 wards streets  $(i, j)$  and  $(i, k)$ . The street  $(g, i)$  is unspoiled, as it is shielded from  
250 the wind that blows through the source of pollution. According to this scheme,  
251 the concentration at the beginning of streets  $(i, j)$  and  $(i, k)$  is the one at the  
252 end of street  $(s, i)$ .

### 253 3. A network perspective

254 In the model presented above, toxic substances move in the urban environ-  
255 ment driven by the wind blowing along the street canyons. The street canyons  
256 behave like upward leaking transport channels and their geometry, position and  
257 connectivity strongly influence the propagation. In big cities, streets cross each  
258 other to compose intricate patterns (Fig. 2). Given the spatial extent and the  
259 high number of elements, these urban fabrics can be seen as complex networks  
260 (Porta et al., 2006; Barthélemy, 2011). Links stand for the street canyons,  
261 while nodes represent the street intersections. The direction and the weight  
262 of the links describe the geometric and fluid-dynamics properties of the street  
263 canyons. Within this approach, the tools of network theory provide interesting  
264 information about the propagation phenomena.

#### 265 3.1. Construction of the network

266 The urban canopy is modelled as a network of  $N$  nodes (intersections) and  
267  $M$  links (streets). Fictitious nodes can be created to divide a street into two  
268 links in case there is a significant change in the street properties. Each link is  
269 directed according to the orientation of the mean wind along the street  $(u_{st})$ .  
270 Thus, the network structure represents both the topological properties of the  
271 urban fabric and the directions in which the propagation processes take place.  
272 The connectivity of the street canyons is described by the adjacency matrix  $\mathbf{A}$ ,  
273 a  $N \times N$  square matrix whose element  $A_{ij}$  is equal to 1 if a directed link from

274 node  $i$  to node  $j$  exists, is equal to 0 otherwise (see Appendix C for an example  
 275 of adjacency matrix). Since the links have a specific direction, the adjacency  
 276 matrix is asymmetric.

277 According to this network representation, the geometry and fluid-dynamics  
 278 properties of the street canyons are stored efficiently in matrices.  $\mathbf{L}$  and  $\mathbf{H}$  are  
 279 the symmetrical matrices of the length of the streets ( $l$ ) and the average height  
 280 of the buildings overlooking the streets ( $h$ ). The wind velocity along the streets  
 281 ( $u_{st}$ ) and the velocity of the vertical transfer towards the external atmosphere  
 282 ( $u_d$ ) are enclosed in the matrices  $\mathbf{U}$  and  $\mathbf{U}_d$ .

283 As mentioned in the Introduction, the main purpose of this work is to es-  
 284 tablish a methodology for the rapid assessment of urban vulnerability to the  
 285 ground-level release of toxic gases. The vulnerability index ( $V_s$ ) for a generic  
 286 node  $s$  can be defined as the number of people affected by the toxic propaga-  
 287 tion if the release takes place in  $s$ . The adopted network approach and matrix  
 288 notation make it easy to calculate  $V_s$  as follows,

$$V_s = \sum_i^N \sum_j^N D_{ij} P_{ij}, \quad (4)$$

289 where  $\mathbf{P}$  is the matrix that associates at each link  $(i, j)$  the number of inhabitants  
 290 per unit street length and  $\mathbf{D}$  is the matrix that associates at each link  $(i, j)$   
 291 the contaminated length of the street. This last matrix represents the zone of  
 292 influence of the source node. The meaning of this matrix and its construction  
 293 process will be widely described in Subsections 3.2 and 3.3.

294 An interesting advantage of this compact notation is that changes to the  
 295 network properties can be easily implemented. By modifying matrices  $\mathbf{U}$  and  
 296  $\mathbf{U}_d$ , we can simulate different meteorological scenarios, while variations in pop-  
 297 ulation distribution (e.g., differences between weekdays and holidays) can be  
 298 considered by adjusting  $\mathbf{P}$ . Furthermore, new buildings and structural changes  
 299 are included in the model by revising the single elements of  $\mathbf{L}$  and  $\mathbf{H}$ .

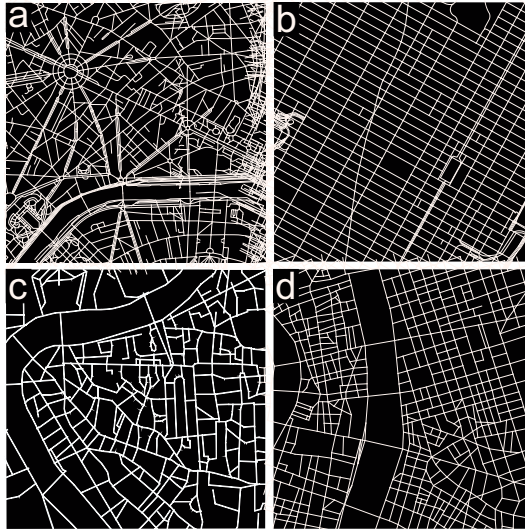


Figure 2: Snapshot of the street network of Paris (a), New York (b), Rome (c), and Lyon (d).

300 *3.2. Propagation of a toxic substance in the street network*

301 Consider the release of a toxic substance in a street intersection (see Fig.  
 302 3.a). According to the hypothesis of our model (Section 2), (i) the substance  
 303 propagates along the adjacent streets depending on the direction of the wind, (ii)  
 304 the concentration decays exponentially along the streets, (iii) the concentration  
 305 at the end of each street can be estimated using (3), (iv) the concentration  
 306 remains unchanged in the street intersections, and (v) from a contaminated  
 307 street intersection the gas spreads further to the adjacent streets.

308 Given this description, the pollutant dispersion within the canopy can be  
 309 then easily seen as a spreading process on a network (e.g., Newman, 2002;  
 310 Comin and da Fontoura Costa, 2011). In Fig. 3.b the urban canopy is rep-  
 311 resented as a network. The links are directed according to the direction of the  
 312 wind in the streets and the release is modelled as a source node  $s$ . From a  
 313 network perspective, transport from  $s$  towards a generic node  $u$  is possible if  
 314 there is a link directed from  $s$  to  $u$ , i.e. if (i) the two nodes are physically con-  
 315 nected by a street canyon, and (ii) the wind is blowing from the source towards  
 316 the target node. Once infected, the target node  $u$  is modelled as a new source

317 and the spreading process carries on towards the farthest nodes. According to  
318 this scheme, propagation is a recursive process that spontaneously expands to  
319 the topological boundaries of the network. Physically, the extent of the con-  
320 taminated zone can be delimited based on a threshold concentration value  $c_{th}$ :  
321 when the concentration falls below  $c_{th}$ , the contamination process is irrelevant.  
322 Thus, a stopping rule for the spreading process on the network is introduced:  
323 at each propagation hop the concentration at the target node is estimated. If  
324 this concentration is higher than  $c_{th}$ , then the propagation carries on.

325 Considering the example in Fig. 3.b, a toxic substance is released in the  
326 source node  $s = 15$  and propagates towards the first neighbours of  $s$ : nodes 10,  
327 11, and 16. The concentration in the first neighbours is evaluated using Equation  
328 (3), as a function of the geometric and wind characteristics of the street canyons  
329 associated to links (15, 10), (15, 11) and (15, 16). Since the concentration in the  
330 first neighbours is greater than the predefined threshold  $c_{th}$ , nodes 10, 11 and  
331 16 act as source nodes and the spreading process carries on towards the second  
332 neighbours of  $s$ . In the same way, the third and fourth neighbours are affected  
333 by the toxic propagation until the concentration in the nodes falls below  $c_{th}$ .

334 According to this network interpretation, the spreading of a toxic gas in  
335 the urban environment is governed by two properties of the network: (i) the  
336 topological connectivity of the network, given by its adjacency matrix  $\mathbf{A}$ , and  
337 (ii) the concentration decay along the links, given by a combination of the  
338 geometric characteristics and the flow dynamics in the street canyons.

339 This spreading results in the zone of influence of the source node  $s$ , i.e.  
340 the set of links contaminated from the propagation process originated in  $s$  (the  
341 elements highlighted in blue in Fig. 3). The number of people that lives in  
342 the zone of influence represents the vulnerability index of  $s$  ( $V_s$ ). Notice that  
343 this index contains both information on population density and meteorological  
344 conditions in the city. In fact, as will be shown in the following sections, its  
345 value changes drastically with the wind direction.



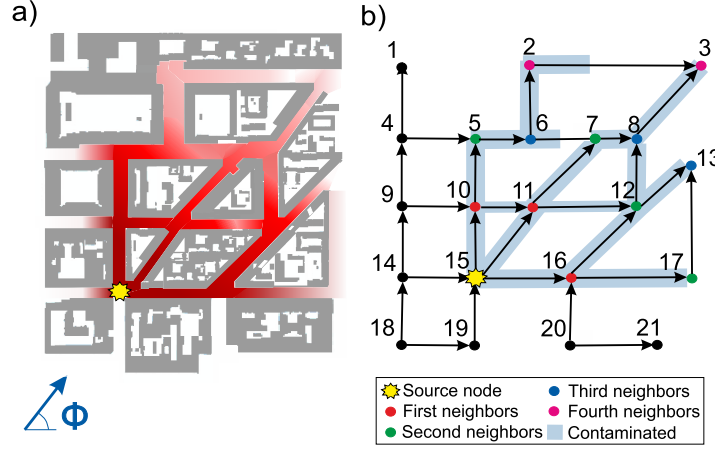


Figure 3: Analogy between the physical propagation of a toxic substance in the urban environment (a) and the spreading process on a network (b).  $\Phi$  is the direction of the external wind blowing on the city.

346 *3.3. Algorithm*

347 Given a source node  $s$  with a concentration  $c_s$ , the set of its first neigh-  
 348 bours  $N_1(s)$  can be derived from the non-zero elements of the  $s$  -  $th$  row of  
 349 the adjacency matrix  $\mathbf{A}$ . In Fig. 3,  $s = 15$  and thus  $N_1(s) = \{10, 11, 16\}$ . For  
 350 each node  $u$  belonging to the set  $N_1(s)$ , the algorithm calculates the distance  
 351  $D_{su}^{pot}$ . This length is the potential distance (hence the superscript *pot*) that the  
 352 contaminated front can reach along the link  $(s, u)$  with a concentration higher  
 353 than the predefined threshold  $c_{th}$ . According to (3),  $D_{su}^{pot}$  is

$$D_{su}^{pot} = -\frac{H_{su}}{U_{d,su}} U_{su} \log\left(\frac{c_{th}}{c_s}\right), \quad \forall u \in N_1(s). \quad (5)$$

354 In general,  $D_{su}^{pot}$  is different from the physical length of the street ( $L_{su}$ ) asso-  
 355 ciated to the link  $(s, u)$ .  $D_{su}^{pot}$  is lower than  $L_{su}$  if the concentration undergoes  
 356 the threshold  $c_{th}$  before the propagation front has travelled the entire street.  
 357 *Vice versa*, it is higher if the front reaches node  $u$  with a concentration above  
 358 the threshold. As a consequence, the effective contaminated distance ( $D_{su}$ ) is  
 359 the minimum between the reachable distance  $D_{su}^{pot}$  and the effective length of

360 the street, i.e.

$$D_{su} = \min[D_{su}^{pot}, L_{su}] \quad (6)$$

361 If  $D_{su} = L_{su}$ , the substance has reached the target node  $u$  with a concen-  
 362 tration equal to or higher than  $c_{th}$ . As a result, node  $u$  is contaminated. Con-  
 363 versely, if the front reaches  $u$  with a negligible concentration (i.e.  $D_{su} < L_{su}$ ),  
 364 then node  $u$  remains unspoiled. In both cases, the algorithm stores the effective  
 365 contaminated length  $D_{su}$  as the  $(s, u)$  element in the matrix  $\mathbf{D}$ . As introduced  
 366 in Section 3.1, this matrix defines the zone of influence of the source node  $s$ .

367 We define  $\hat{N}_1(s)$  the set of the first neighbours of  $s$  that have been contam-  
 368 inated,

$$\hat{N}_1(s) = \{u \in N_1(s) \mid D_{su} = L_{su}\}. \quad (7)$$

369 Referring to Fig. 3,  $\hat{N}_1(15) = \{10, 11, 16\}$  since all the first neighbours of  
 370  $s$  are contaminated. The algorithm estimates the concentration in the nodes  
 371 belonging to  $\hat{N}_1(s)$  using (3), as

$$c_u = c_s e^{-\frac{U_{d,su} L_{su}}{H_{su} U_{su}}}, \quad \forall u \in \hat{N}_1(s). \quad (8)$$

372 These nodes behave as new source nodes. Thus, the algorithm repeats the above  
 373 presented steps, replacing in Equations (5)-(8) node  $s$  with the nodes belonging  
 374 to  $\hat{N}_1(s)$ . For example, once node 16 (Fig. 3) has been contaminated from  
 375 the initial source node 15, the algorithm finds the set of its first neighbours,  
 376 i.e.  $N_1(16) = \{12, 17\}$ . Equations (5)-(6) estimate the effective contaminated  
 377 length along links (16, 12) and (16, 17), while (7) identifies the set of the first  
 378 neighbours of node 16 that have been infected, i.e.  $\hat{N}_1(16) = \{12, 17\}$ . Finally,  
 379 the concentration reached in nodes 12 and 17 is determined by (8). This proce-  
 380 dure is repeated recursively until the concentration in each node of the network  
 381 falls below the threshold  $c_{th}$ .

382 Notice that for nodes 15 and 16 the sets  $N_1$  and  $\hat{N}_1$  are identical. However,

383 this is not true in general. Consider node 6 in Fig. 3b. The set of its first neigh-  
 384 bours is  $N_1(6) = \{2, 7\}$ , while  $\hat{N}_1(6) = \{2\}$  because node 7 cannot be reached  
 385 by the propagation along link (6, 7).

386

387 The algorithm explores the nodes of the network starting from a root node  
 388 and progressively visiting the adjacent nodes. In computer science, this process  
 389 is called tree traversal (Valiente, 2013) since the result of the exploration is a  
 390 tree structure that is a subgraph of the initial graph. In our study, this tree  
 391 corresponds to the zone of influence of the source node. There are multiple  
 392 ways to perform a tree traversal, according to the order in which the nodes are  
 393 visited. The algorithm presented above explores the nodes of the network using  
 394 a depth-first search analysis. The algorithm starts at the source node and goes  
 395 as far as it can down a given branch before backtracking. Referring to Fig.  
 396 3, the algorithm starts at node 15, selects the first node 10 in the set  $\hat{N}_1(15)$   
 397 and deepens the analysis in the first element of the set  $\hat{N}_1(10)$ , i.e. node 5.  
 398 Following this ratio, the algorithm visits the nodes in the order (15, 10, 5, 6, 2).  
 399 The in-depth analysis along this path ends when the concentration falls below  
 400 the threshold  $c_{th}$ . Formally, the path (15, 10, 5, 6, 2) ends because the set  $\hat{N}_1(2)$   
 401 is empty. Once the first branch has been explored, the algorithm backtracks to  
 402 node 6's next available neighbour, i.e. node 7.

403 From the numerical point of view, depth-first search analysis requires less  
 404 memory and it is more efficient in finding trees on networks compared to other  
 405 algorithms, such as breath-first search (Kozen, 1992).

406 Notice that, referring to the example in Fig. 3b, link (11, 7) is affected  
 407 by toxic propagation twice, both along propagation path  $\gamma_1=(15, 11, 7)$  and  
 408  $\gamma_2=(15, 10, 11, 7)$ . As a consequence the algorithm calculates two different  
 409 values of  $D_{11,7}$ , since the concentration reached at node 11 ( $c_{11}$ ) along  $\gamma_1$  is  
 410 generally different from the one obtained along  $\gamma_2$ . As the aim of the elaboration  
 411 is to determine the extent of the zone of influence, the algorithm considers all the  
 412 possible passages through a generic link and stores the longest distance reached  
 413 by the toxic substance. In details, for each path  $\gamma_\alpha$  the algorithm compares

414  $D_{su}^{(\gamma_\alpha)}$  with the distance  $D_{su}^{(\gamma_{\alpha-1})}$  obtained along the previously explored path  
415  $\gamma_{\alpha-1}$  passing through the link  $(s, u)$ . Equation (6) is, thus, refined as:

$$D_{su}^{(\gamma_\alpha)} = \max[\min[D_{su}^{pot}, L_{su}], D_{su}^{(\gamma_{\alpha-1})}], \quad (9)$$

416 where  $\gamma_\alpha$  is an index for the order in which the path is explored.

#### 417 **4. Results**

418 The potentials of the proposed approach are discussed through a case study.  
419 The model is applied to assess urban vulnerability of the city of Lyon (France)  
420 to the release of a toxic gas. Lyon (Fig. 4) is located in east-central France and  
421 it is the third-largest urban agglomeration in France after Paris and Marseille,  
422 with a population of approximately 1.5 million inhabitants. In this work, the  
423 analysis is limited to a part of the city (Fig. 4c) that presents an intricate urban  
424 fabric and tall buildings on the edge of the streets. These characteristics are  
425 consistent with the model representation of the streets as a network of street  
426 canyons. The study area has an extent of about  $6.5 \text{ km}^2$ , it hosts a population of  
427 about 140,000 inhabitants and is delimited by natural and artificial boundaries  
428 (rivers, parks and railways). These boundaries determine a discontinuity in the  
429 dispersion of pollutants along the street canyons.

430 The street canyons and the street intersections result in a network of 750  
431 nodes and 1110 links. The geometric characteristics of the street canyons, the  
432 population density, the longitudinal mean wind and the vertical transfer velocity  
433 in the streets are stored in the matrices  $\mathbf{H}$ ,  $\mathbf{L}$ ,  $\mathbf{P}$ ,  $\mathbf{U}$  and  $\mathbf{U}_d$ , respectively.

##### 434 *4.1. The zone of influence of a source node*

435 The first outcome of the elaboration is the identification of the zone of influ-  
436 ence of a source node, i.e. the set of links contaminated by the toxic substance  
437 with a concentration above a defined threshold, stored in matrix  $\mathbf{D}$  (see Section  
438 3).

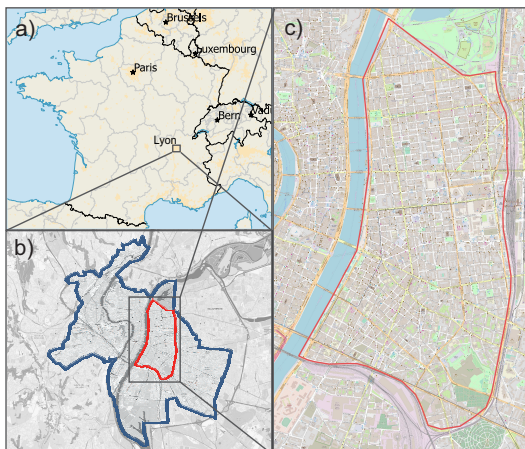


Figure 4: The case study area. a) Location of the metropolitan area of Lyon within France. b) Location of the study area within the municipality of Lyon. c) The study area.

439 As an example, Fig. 5 shows the zone of influence of a source node for differ-  
 440 ent wind directions ( $\Phi = 45^\circ, 135^\circ, 225^\circ$  and  $315^\circ$ ) and for two different initial  
 441 concentration values. For the sake of generality, the concentration scenarios are  
 442 defined by the ratio between the concentration in the source node ( $c_0$ ) and the  
 443 limit concentration ( $c_{th}$ ).

444 The urban topology, the wind direction and the initial concentration shape  
 445 the zone of influence of the source node. Variations in the mean velocity of  
 446 the external wind ( $\bar{u}$ ) as well as the stability conditions (as determined by the  
 447 Monin-Obukhov length  $L_{MO}$ ) are instead irrelevant. As stated in (2) and (A.1)-  
 448 (A.2), both  $u_d$  and  $u_{st}$  linearly depend on the friction velocity  $u_*$ . Since our  
 449 propagation model evaluates the pollutant spreading as a function of their ratio  
 450 (3), variations of  $u_*$ , and thus of  $L_{MO}$  and  $\bar{u}$ , will not be effective in determining  
 451 the zone of influence.

#### 452 4.2. Spatial and frequency distribution of urban vulnerability

453 The spatial pattern of urban vulnerability can be analysed at a glance using  
 454 vulnerability maps. Given the geometry of the urban fabric, the conditions  
 455 of the external wind, the spatial distribution of the citizens and the emission  
 456 scenario, the model provides in a short time (from a few seconds to a few minutes

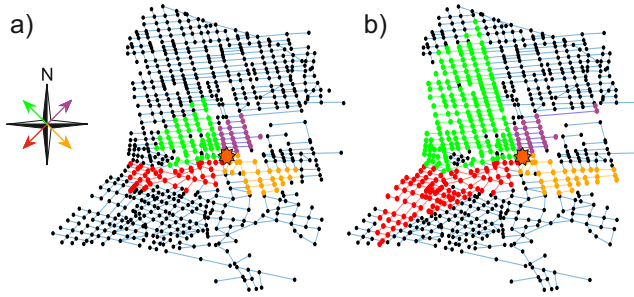


Figure 5: The zone of influence of a generic source node (orange star) in the network for different wind directions (red, green, violet and yellow refer to the wind directions  $\Phi = 45^\circ$ ,  $135^\circ$ ,  $225^\circ$  and  $315^\circ$ , respectively). Panel (a) and (b) refer to a concentration ratio  $c_0/c_{th} = 10$  and  $c_0/c_{th} = 100$ , respectively.

457 depending on the concentration ratio  $c_0/c_{th}$ ) a map that associates at each node  
 458 of the street network its vulnerability index. To do this, the algorithm for the  
 459 spread of toxic substances on networks (Section 3) is applied and the matrix of  
 460 the contaminated street lengths  $\mathbf{D}$  (i.e. the zone of influence) is computed for all  
 461 nodes of the network. Next, the vulnerability index defined in Equation (4) is  
 462 calculated for each node, taking into account both the extent of the zone affected  
 463 by the propagation originated in the node ( $\mathbf{D}$ ) and the number of people leaving  
 464 in that zone ( $\mathbf{P}$ ). Finally, a vulnerability map is constructed by associating a  
 465 colour to each node based on its vulnerability index.

466 Sixteen vulnerability maps for the case study area are obtained (see the  
 467 supplementary material) by varying the direction of the external wind ( $\Phi$ ) and  
 468 the concentration ratio  $c_0/c_{th}$ . These parameters affect the node vulnerability  
 469 by shaping its zone of influence (matrix  $\mathbf{D}$ ), as mentioned in Section 4.1. In  
 470 this study, the number of inhabitants in the streets ( $\mathbf{P}$ ) was kept constant in  
 471 the different scenarios and was derived from the map of the resident citizens in  
 472 the city of Lyon. Future works should consider how the spatial distribution of  
 473 the population varies on different days of the week or at different times of the  
 474 day. These variations could be easily implemented in the model by modifying  
 475 the  $\mathbf{P}$  matrix and would increase the number of cases (i.e. maps) considered.

476 Fig. 6 shows four vulnerability maps for a wind direction varying between  
 477  $\Phi = 0^\circ$  (north wind) and  $\Phi = 135^\circ$ . The maps are obtained simulating for

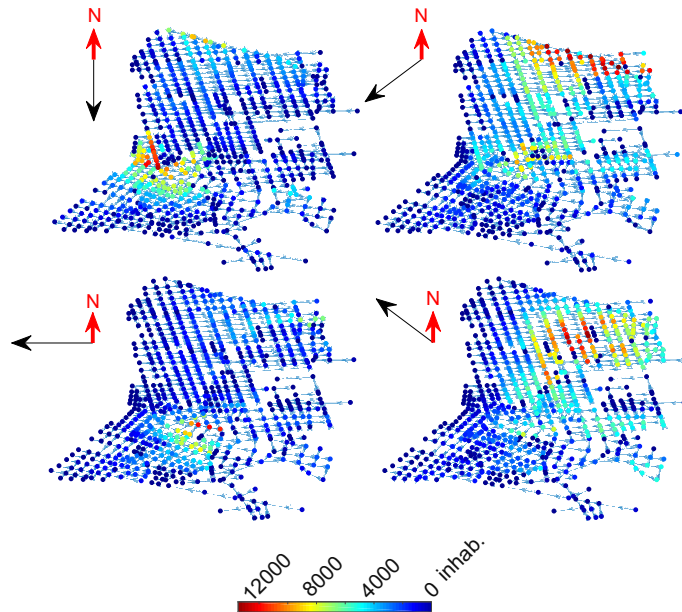


Figure 6: Vulnerability maps for different wind directions and with a concentration ratio  $c_0/c_{th}$  equal to 10.

478 each node a release with a concentration equal to ten times the threshold value,  
 479 i.e.  $c_0/c_{th} = 10$ . Node vulnerability, defined in terms of affected people, varies  
 480 between 0 (blue) and 12000 (red) inhabitants. The maps reveal at a glance  
 481 the most susceptible areas and the global vulnerability of the urban fabric in  
 482 the different wind direction scenarios. From Fig. 6, it can be seen that the  
 483 vulnerability index is not distributed homogeneously. On the contrary, the  
 484 vulnerability tends to be maximal (red nodes) in a defined area of the map and  
 485 its value gradually decreases in the nodes around it. Moreover, the position  
 486 of the most vulnerable nodes varies strongly with small variations in the wind  
 487 direction. As an example, notice the difference between the two scenarios related  
 488 to  $\Phi = 0^\circ$  and  $\Phi = 45^\circ$  in Fig. 6.

489 To better understand this behaviour, Fig. 7.a summarizes the results of the  
 490 sixteen simulated scenarios. Each scenario is represented by an arrow oriented  
 491 with the wind direction, coloured according to the concentration ratio and po-  
 492 sitioned in the area of greatest vulnerability for that scenario. It is evident that

493 for  $\Phi$  equal to  $0^\circ$ ,  $90^\circ$ ,  $180^\circ$  and  $270^\circ$  (the cardinal directions) the most vulner-  
 494 able nodes are located in the southern part of the network, while for  $\Phi$  equal to  
 495  $45^\circ$ ,  $135^\circ$ ,  $225^\circ$  and  $315^\circ$  (the transversal directions) the most vulnerable areas  
 496 are in the northern part of the network.

497 As the geometric characteristics of the street canyons and the population  
 498 density are rather homogeneously distributed in the street network, this differ-  
 499 ent vulnerability pattern is related to the orientation of the streets with respect  
 500 to the wind direction. The northern part of the street network is mainly ori-  
 501 ented according to the cardinal directions (North-South and West-East oriented  
 502 streets). As the wind blows in one of these directions (e.g.,  $\Phi = 0^\circ$ ), only the  
 503 aligned streets (i.e. the North-South oriented streets) are affected by the prop-  
 504 agation of toxic substances, while the orthogonal streets (i.e. the East-West  
 505 oriented streets) are completely shielded from the wind. This condition limits  
 506 the extent of the zone of influence of a generic source node. Conversely, as the  
 507 wind blows according to one of the transversal direction, the propagation affects  
 508 both the North-South and the East-West oriented streets, thus increasing the  
 509 vulnerability. As the southern part of the street network is oriented mainly  
 510 according to the transverse directions, a greater vulnerability will occur when  
 511 the wind is blowing in the cardinal directions.

512 For each of the sixteen scenarios analysed, the average vulnerability over the  
 513 entire network ( $\bar{V}$ ) is calculated as

$$\bar{V} = \frac{1}{N} \sum_i^N V_i, \quad (10)$$

514 where  $V_i$  is the vulnerability index for the  $i$ -th node and  $N$  is the number of  
 515 nodes in the network. The two polar histograms of Fig. 7.b report these average  
 516 vulnerability values for the two concentration ratios considered. Each sector in  
 517 the polar histograms refers to a different wind direction. As expected, higher  
 518 concentration ratios correspond to higher vulnerability values. Moreover, since  
 519 most of the streets ( $\sim 60\%$ ) are oriented in the cardinal directions, the average  
 520 vulnerability is greater when the wind blows in the transversal directions.



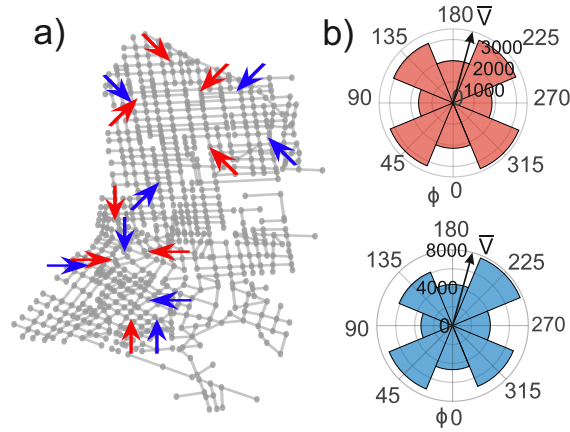


Figure 7: a) Most vulnerable areas in the street network for different wind directions and concentration ratios. Each scenario is represented by an arrow oriented according to the wind direction, coloured according to the concentration ratio (red arrows for  $c_0/c_{th} = 10$  and blue arrows for  $c_0/c_{th} = 100$ ) and positioned in the area of greatest vulnerability on the map. b) Polar histogram (red for  $c_0/c_{th} = 10$  and blue for  $c_0/c_{th} = 100$ ) of the average node vulnerability for the different wind directions

521 Fig. 8 gives an overview of the long-term vulnerability of the urban fabric  
 522 to toxic releases. The maps depict nodes vulnerability weighted by the annual  
 523 frequency of the wind directions over the city of Lyon. As detailed in the inset of  
 524 Fig. 8, the dominant wind direction in Lyon is North-South. As a consequence,  
 525 the highest vulnerabilities are located in the circled area, corresponding to the  
 526 regions mostly stressed by North-South oriented winds (see  $\Phi = 0^\circ$  and  $\Phi = 180^\circ$   
 527 scenarios in the supplementary material).

528 Results in Fig. 6 suggest that, for each scenario, a restricted area of the  
 529 urban fabric is characterized by high levels of vulnerability, while most of the  
 530 streets are not exposed. Thus, both spatial and frequency distribution of node  
 531 vulnerabilities are not trivial. A frequency analysis of vulnerability values was  
 532 performed to identify an eventual significant statistical distribution of the data.  
 533 For each scenario, node vulnerability values were classified in ten equal size  
 534 intervals. Then, the relative frequency ( $p$ ) of each class was calculated. Fig. 9

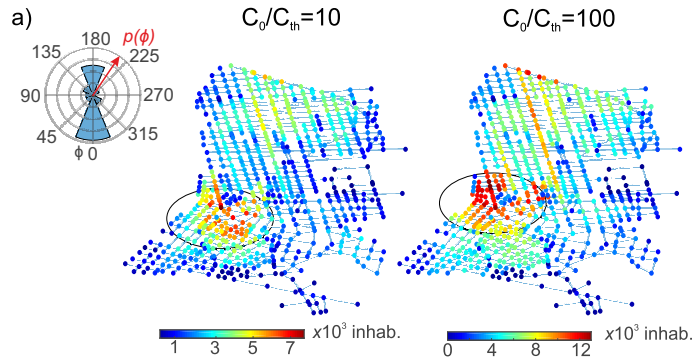


Figure 8: Maps of vulnerability weighted by the annual frequency of the wind directions. The polar histogram (inset *a*) shows the occurrence of wind directions in the city of Lyon in terms of annual relative frequency  $p(\Phi)$ .

535 presents the relative frequency of node vulnerability for the different scenarios  
 536 in a log-log plot. For the sake of graphic clarity, vulnerability values were  
 537 normalised to the maximum one ( $V_{max}$ ). Generally, the data show a linear  
 538 behaviour in the log-log plot, thus exhibiting a power law trend. The power law  
 539 confirms that vulnerability distribution is heterogeneous, with few nodes being  
 540 much more critical than the others. This hierarchical configuration suggests  
 541 that, for each wind scenario, the entire neighbourhood could be protected with  
 542 security interventions targeted on small urban areas.

543 Notice that many real-world networks (e.g., the Internet, World Wide Web,  
 544 scientific citations) present a power law distribution of nodes degree (Boccaletti  
 545 et al., 2006). The degree defines the importance of a node in the network  
 546 in terms of its connectivity. In this case, a power law results from the not  
 547 trivial interaction of multiple factors that define the vulnerability index, i.e.  
 548 the topological connectivity of the network, the geometry characteristics of the  
 549 street canyons, the toxic spreading process and the population distribution in  
 550 the city.

## 551 5. Conclusions

552 We have presented an innovative approach for the study of diffusion pro-  
 553 cesses in the urban atmosphere. Within the urban canopy, the wind flows along

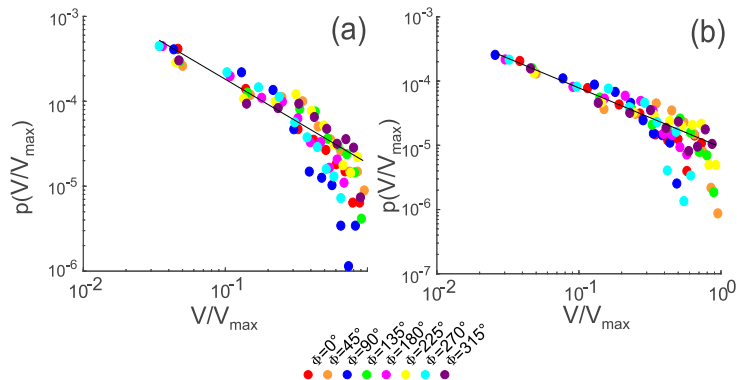


Figure 9: Relative frequency of vulnerability for different wind directions and for a concentration ratio  $c_0/c_{th} = 10$  (a) and  $c_0/c_{th} = 100$  (b). The display is in logarithmic scale.

554 the street canyons and the transport of pollutants is strongly influenced by the  
 555 structure of the city, i.e. by the orientation of the streets and by their intercon-  
 556 nections. Moving from these considerations, we have modelled the interaction  
 557 between the city and the external wind as a weighted complex network whose  
 558 links and nodes represent the streets and the street intersections, respectively.  
 559 The direction of the links and their weights describe the direction and the inten-  
 560 sity of the wind along the streets and the geometric properties of the buildings  
 561 that surround the street canyons. Using a depth-first search analysis, we have  
 562 implemented a spreading model on networks that simulates the propagation  
 563 process from a point source. As an example, the developed method has been  
 564 adopted to create vulnerability maps of the city of Lyon (France). These maps  
 565 highlight the most vulnerable areas of the city, i.e. the areas from which the  
 566 spread of a toxic substance, released at ground level, can damage more people.  
 567 We found that the spatial and frequency distribution of urban vulnerability is  
 568 heterogeneous and is strongly influenced by the alignment between the direction  
 569 of the external wind and the orientation of the streets.

570 The model proved to be quick and functional and therefore useful for the  
 571 analysis of multiple scenarios that take into account various meteorological con-  
 572 ditions or different distributions of the residing population. Thanks to these  
 573 characteristics, this method is suitable for the prediction and management of

574 emergency scenarios, due to accidental or harmful releases of toxic substances  
 575 in the urban atmosphere.

576 This work is in line with recent efforts to develop operational modelling tools  
 577 for the prediction of pollutant transport in large urban areas. Moreover, the  
 578 study demonstrate that the innovative tools of the theory of complex networks  
 579 can be adopted to this aim. The frequency with which new techniques and  
 580 applications are developed in the field of complex networks makes this new  
 581 perspective particularly promising.

582 Future work is aimed at comparing different cities to understand how urban  
 583 topology influences the diffusive process and therefore the vulnerability of the  
 584 city. In this way, it will be possible to understand which cities are the most  
 585 structurally fragile. Further analyses should be conducted to consider variations  
 586 in urban vulnerability due to changes in the presence of people in the different  
 587 times of the day or during the different periods of the week. Finally, the results  
 588 encourage a deeper understanding of the link between the theory of complex  
 589 networks and the problems of diffusion in the urban environment.

## 590 **Appendix A. Longitudinal wind velocity along a street canyon**

591 According to Soulhac et al. (2008), the average velocity  $u_{st}$  along the longi-  
 592 tudinal axis of a street canyon reads

$$\begin{aligned}
 u_{st} = u_H \cos \Phi \frac{\delta_i^2}{hw} & \left[ \frac{2\sqrt{2}}{C} (1 - \beta) \left( 1 - \frac{C^2}{3} + \frac{C^4}{45} \right) + \beta \frac{2\alpha - 3}{\alpha} \right. \\
 & \left. + \left( \frac{w}{\delta_i} - 2 \right) \frac{\alpha - 1}{\alpha} \right] \tag{A.1}
 \end{aligned}$$

$$\text{with} = \begin{cases} \alpha = \ln \left( \frac{\delta_i}{z_{0,build}} \right) \\ \beta = \exp \left[ \frac{C}{\sqrt{2}} \left( 1 - \frac{h}{\delta_i} \right) \right] \\ u_H = u_* \sqrt{\frac{\pi}{\sqrt{2}k^2 C} \left[ Y_0(C) - \frac{J_0(C)Y_1(C)}{J_1(C)} \right]} \\ C \text{ solution of } \frac{z_{0,build}}{\delta_i} = \frac{2}{C} \exp \left[ \frac{\pi}{2} \frac{Y_1(C)}{J_1(C)} - \gamma \right] \\ \delta_i = \min \left( h, \frac{w}{2} \right) \end{cases} \quad (\text{A.2})$$

593 where  $\Phi$  is the external wind direction with respect to the street longitudinal  
594 axis,  $h$  and  $w$  are the height and the width of the street canyon,  $z_{0,build}$  is  
595 the aerodynamic roughness of the canyon walls,  $u_*$  is the friction velocity of the  
596 external atmospheric boundary layer flow,  $J_0$ ,  $J_1$ ,  $Y_0$  and  $Y_1$  are Bessel functions,  
597  $k$  is the von Kármán constant, and  $\gamma$  is the Euler constant. The friction velocity  
598  $u_*$  is determined using the Monin-Obukhov similarity theory to model the flow  
599 in the external boundary layer.

## 600 Appendix B. Solution for the one-dimensional transport equation

601 Under the assumption that  $c_{ext}$  is negligible with respect to the concentration  
602 in the street canyon, the one-dimensional transport equation (1) becomes

$$\frac{\partial c}{\partial t} + u_{st} \frac{\partial c}{\partial x} + \frac{u_d}{h} c = 0. \quad (\text{B.1})$$

603 By introducing the substitution

$$g(x, t) = c(x, t) \exp \left( \frac{u_d}{h} t \right), \quad (\text{B.2})$$

604 (B.1) yields

$$\frac{\partial g}{\partial t} + u_{st} \frac{\partial g}{\partial x} = 0. \quad (\text{B.3})$$

605 The general solution for (B.3) is found by introducing the new coordinates  
606  $\tau = t$ ,  $\xi = x - u_{st}t$  and using the chain rule:

$$\frac{\partial g(x, t)}{\partial t} = \frac{\partial g(\xi, \tau)}{\partial \tau} - u_{st} \frac{\partial g(\xi, \tau)}{\partial \xi} \quad (\text{B.4})$$

$$\frac{\partial g(x, t)}{\partial x} = \frac{\partial g(\xi, \tau)}{\partial \xi}. \quad (\text{B.5})$$

607 Equation (B.3) becomes

$$\frac{\partial g(\xi, \tau)}{\partial \tau} = 0, \quad (\text{B.6})$$

608 and, therefore,

$$g(\xi, \tau) = F(\xi) \quad \rightarrow \quad g(x, t) = F(x - u_{st}t), \quad (\text{B.7})$$

609 where  $F$  is a derivable function. The solution of (B.1) is obtained returning to  
610 the original function,

$$c(x, t) = g(x, t) \exp\left(-\frac{u_d}{h}t\right) = F(x - u_{st}t) \exp\left(-\frac{u_d}{h}t\right). \quad (\text{B.8})$$

611 Function  $F$  is found using the initial or boundary conditions of the problem.

612 For a continuous release  $c_0$  in the source node starting from  $t \geq 0$ , the  
613 boundary condition is defined as

$$c(0, t) = c_0 \Theta(t), \quad (\text{B.9})$$

614 where  $\Theta$  is the Heaviside function. For  $x = 0$ , (B.8) and (B.9) yield

$$c(0, t) = F(-u_{st}t) \exp\left(-\frac{u_d}{h}t\right) = c_0 \Theta(t). \quad (\text{B.10})$$

615 Function  $F$  is obtained from the previous one and the solution for the continuous  
616 release is thus

$$c(x, t) = F(x - u_{st}t) \exp\left(-\frac{u_d}{h}t\right) = c_0 \exp\left(-\frac{u_d}{u_{st}h}x\right) \Theta\left(t - \frac{x}{u_{st}}\right). \quad (\text{B.11})$$

617 For a quick release in the source node, the initial condition is set as a rect-  
 618 angular pulse with width  $a$  and height  $c_0$

$$c(x, 0) = c_0[\Theta(x) - \Theta(x - a)]. \quad (\text{B.12})$$

619 When  $a$  tends to zero, the release is almost instantaneous. Following the same  
 620 reasoning as in (B.10) and (B.11), but considering this time  $t = 0$ , we obtain  
 621 the solution for a quick release:

$$c(x, t) = c_0 \exp\left(-\frac{u_d}{h}t\right) [\Theta(x - u_{st}t) - \Theta(x - u_{st}t - a)]. \quad (\text{B.13})$$

## 622 Appendix C. Adjacency matrix

623 Consider the network in Fig.1c, extracted as a subgraph from the network  
 624 of streets in Fig.1a. The adjacency matrix of this simple four-links graph reads

$$\mathbf{A} = \begin{matrix} & \begin{matrix} s & g & i & j & k \end{matrix} \\ \begin{matrix} s \\ g \\ i \\ j \\ k \end{matrix} & \begin{pmatrix} 0 & 0 & 1 & 0 & 0 \\ 0 & 0 & 1 & 0 & 0 \\ 0 & 0 & 0 & 1 & 1 \\ 0 & 0 & 0 & 0 & 0 \\ 0 & 0 & 0 & 0 & 0 \end{pmatrix} \end{matrix}. \quad (\text{C.1})$$

625 Note that the matrix is asymmetric since the network is directed (i.e. the links  
 626 have a specific direction).

## 627 References

- 628 Ahern, J., 2011. From fail-safe to safe-to-fail: Sustainability and resilience in  
 629 the new urban world. *Landscape and Urban Planning* 100 (4), 341–343.
- 630 Arnfield, A. J., 2003. Two decades of urban climate research: A review of turbu-  
 631 lence, exchanges of energy and water, and the urban heat island. *International*  
 632 *Journal of Climatology* 23 (1), 1–26.

- 633 Barthélemy, M., 2011. Spatial networks. *Physics Reports* 499 (1-3), 1–101.
- 634 Berke, P. R., Song, Y., Stevens, M., 2009. Integrating hazard mitigation into  
635 new urban and conventional developments. *Journal of Planning Education*  
636 and Research 28 (4), 441–455.
- 637 Blocken, B., 2015. Computational Fluid Dynamics for urban physics: Impor-  
638 tance, scales, possibilities, limitations and ten tips and tricks towards accurate  
639 and reliable simulations. *Building and Environment* 91, 219–245.
- 640 Boccaletti, S., Latora, V., Moreno, Y., Chavez, M., Hwang, D.-U., 2006. Com-  
641 plex networks: Structure and dynamics. *Physics Reports* 424 (4-5), 175–308.
- 642 Borgatti, S. P., Mehra, A., Brass, D. J., Labianca, G., 2009. Network analysis  
643 in the social sciences. *Science* 323 (5916), 892–895.
- 644 Brunekreef, B., Holgate, S. T., 2002. Air pollution and health. *The Lancet*  
645 360 (9341), 1233–1242.
- 646 Carruthers, D., Edmunds, H., Lester, A., McHugh, C., Singles, R., 2000. Use  
647 and validation of ADMS-Urban in contrasting urban and industrial locations.  
648 *International Journal of Environment and Pollution* 14 (1-6), 364–374.
- 649 Carvalho, R., Buzna, L., Bono, F., Gutiérrez, E., Just, W., Arrowsmith, D.,  
650 2009. Robustness of trans-European gas networks. *Physical Review E* 80 (1),  
651 016106.
- 652 Comin, C. H., da Fontoura Costa, L., 2011. Identifying the starting point of a  
653 spreading process in complex networks. *Physical Review E* 84 (5), 056105.
- 654 Di Sabatino, S., Buccolieri, R., Salizzoni, P., 2013. Recent advancements in  
655 numerical modelling of flow and dispersion in urban areas: A short review.  
656 *International Journal of Environment and Pollution* 7 52 (3-4), 172–191.
- 657 Gelbrecht, M., Boers, N., Kurths, J., 2017. A complex network representation of  
658 wind flows. *Chaos: An Interdisciplinary Journal of Nonlinear Science* 27 (3),  
659 035808.



- 660 Giustolisi, O., Ridolfi, L., 2014. A novel infrastructure modularity index for  
661 the segmentation of water distribution networks. *Water Resources Research*  
662 50 (10), 7648–7661.
- 663 Heinrich, J., Wichmann, H.-E., 2004. Traffic related pollutants in Europe and  
664 their effect on allergic disease. *Current Opinion in Allergy and Clinical Im-*  
665 *munology* 4 (5), 341–348.
- 666 Hunter, L. J., Watson, I., Johnson, G., 1990. Modelling air flow regimes in urban  
667 canyons. *Energy and Buildings* 15 (3-4), 315–324.
- 668 Kozen, D. C., 1992. Depth-first and breadth-first search. In: *The Design and*  
669 *Analysis of Algorithms*. Springer, pp. 19–24.
- 670 Mayer, H., 1999. Air pollution in cities. *Atmospheric Environment* 33 (24-25),  
671 4029–4037.
- 672 McLeish, C., 2017. Recasting the threat of chemical terrorism in the EU: The is-  
673 sue of returnees from the syrian conflict. *European Journal of Risk Regulation*  
674 8 (4), 643–657.
- 675 Namdeo, A., Colls, J., 1996. Development and evaluation of SBLINE, a suite of  
676 models for the prediction of pollution concentrations from vehicles in urban  
677 areas. *Science of the Total Environment* 189, 311–320.
- 678 Newman, M., 2010. *Networks: An introduction*. Oxford university press.
- 679 Newman, M. E., 2002. Spread of epidemic disease on networks. *Physical Review*  
680 E 66 (1), 016128.
- 681 Oke, T. R., 1982. The energetic basis of the urban heat island. *Quarterly Journal*  
682 *of the Royal Meteorological Society* 108 (455), 1–24.
- 683 Porta, S., Crucitti, P., Latora, V., 2006. The network analysis of urban streets:  
684 A dual approach. *Physica A: Statistical Mechanics and its Applications*  
685 369 (2), 853–866.

- 686 Robins, A., Savory, E., Scaperdas, A., Grigoriadis, D., 2002. Spatial variability  
687 and source-receptor relations at a street intersection. *Water, Air and Soil*  
688 *Pollution: Focus 2* (5-6), 381–393.
- 689 Roth, M., 2000. Review of atmospheric turbulence over cities. *Quarterly Journal*  
690 *of the Royal Meteorological Society* 126 (564), 941–990.
- 691 Salizzoni, P., Soulhac, L., Mejean, P., 2009. Street canyon ventilation and at-  
692 mospheric turbulence. *Atmospheric Environment* 43 (32), 5056–5067.
- 693 Ser-Giacomi, E., Rossi, V., López, C., Hernandez-Garcia, E., 2015. Flow net-  
694 works: A characterization of geophysical fluid transport. *Chaos: An Interdis-*  
695 *ciplinary Journal of Nonlinear Science* 25 (3), 036404.
- 696 Soulhac, L., Garbero, V., Salizzoni, P., Mejean, P., Perkins, R., 2009. Flow and  
697 dispersion in street intersections. *Atmospheric Environment* 43 (18), 2981–  
698 2996.
- 699 Soulhac, L., Perkins, R. J., Salizzoni, P., 2008. Flow in a street canyon for any  
700 external wind direction. *Boundary-Layer Meteorology* 126 (3), 365–388.
- 701 Soulhac, L., Salizzoni, P., Cierco, F.-X., Perkins, R., 2011. The model SIRANE  
702 for atmospheric urban pollutant dispersion; part I, presentation of the model.  
703 *Atmospheric Environment* 45 (39), 7379–7395.
- 704 Soulhac, L., Salizzoni, P., Mejean, P., Perkins, R., 2013. Parametric laws to  
705 model urban pollutant dispersion with a street network approach. *Atmo-*  
706 *spheric Environment* 67, 229–241.
- 707 Tominaga, Y., Stathopoulos, T., 2012. CFD modeling of pollution dispersion in  
708 building array: Evaluation of turbulent scalar flux modeling in RANS model  
709 using LES results. *Journal of Wind Engineering and Industrial Aerodynamics*  
710 104, 484–491.
- 711 Tucker, J. B., 2000. *Toxic terror: Assessing terrorist use of chemical and bio-*  
712 *logical weapons*. MIT Press.

- 713 Valiente, G., 2013. Algorithms on trees and graphs. Springer Science & Business  
714 Media.
- 715 Yazdani, A., Jeffrey, P., 2011. Complex network analysis of water distribution  
716 systems. Chaos: An Interdisciplinary Journal of Nonlinear Science 21 (1),  
717 016111.

**Supplementary Material**

[Click here to download Supplementary Material: Supplementary\\_material.pdf](#)